

OSTEOGENIC DIFFERENTIATION OF HUMAN DENTAL PULP STEM CELLS IN DECELLULARISED ADIPOSE TISSUE SOLID FOAMS

J. Luzuriaga¹, P. García-Gallastegui¹, N. García-Urki², J.R. Pineda^{1,3}, I. Irastorza¹, F.-J. Fernandez-San-Argimiro², N. Briz², B. Olalde², F. Unda¹, I. Madarieta² and G. Ibarretxe^{1,*}

¹ Department of Cell Biology and Histology, Faculty of Medicine and Nursing, University of the Basque Country, UPV/EHU, Leioa, 48940, Bizkaia, Spain

² TECNALIA, Basque Research and Technology Alliance (BRTA), E20009, Donostia-San Sebastian, Spain

³ Achucarro Basque Centre for Neuroscience Fundazioa, Leioa, 48940, Bizkaia, Spain

Abstract

3D cell culture systems based on biological scaffold materials obtainable from both animal and human tissues constitute very interesting tools for cell therapy and personalised medicine applications. The white adipose tissue (AT) extracellular matrix (ECM) is a very promising biomaterial for tissue engineering due to its easy accessibility, malleability and proven biological activity. In the present study, human dental pulp stem cells (hDPSCs) were combined *in vitro* with ECM scaffolds from porcine and human decellularised adipose tissues (pDAT, hDAT) processed as 3D solid foams, to investigate their effects on the osteogenic differentiation capacity and bone matrix production of hDPSCs, compared to single-protein-based 3D solid foams of collagen type I and conventional 2D tissue-culture-treated polystyrene plates. pDAT solid foams supported the osteogenic differentiation of hDPSCs to similar levels to collagen type I, as assessed by alkaline phosphatase and alizarin red stainings, reverse transcription quantitative real-time polymerase chain reaction (RT-qPCR) and osteocalcin/bone gamma-carboxyglutamate protein (BGLAP) immunostaining. Interestingly, hDAT solid foams showed a markedly lower capacity to sustain hDPSC osteogenic differentiation and matrix calcification and a higher capacity to support adipogenesis, as assessed by RT-qPCR and oil red O staining. White ATs from both human and porcine origins are relatively abundant and available sources of raw material to obtain high quality ECM-derived biomedical products. These biomaterials could have promising applications in tissue engineering and personalised clinical therapy for the healing and regeneration of lesions involving not only a loss of calcified bone but also its associated soft non-calcified tissues.

Keywords: Dental pulp stem cells, adipose tissue, bone tissue, extracellular matrix, decellularisation, solid foam, osteogenic differentiation, mineralisation.

* **Address for correspondence:** Gaskon Ibarretxe, Department of Cell Biology and Histology, Faculty of Medicine and Nursing, University of the Basque Country, UPV/EHU, Leioa, 48940, Bizkaia, Spain. Telephone number: +34 946013218 Email: gaskon.ibarretxe@ehu.eus

Copyright policy: This article is distributed in accordance with Creative Commons Attribution Licence (<http://creativecommons.org/licenses/by/4.0/>).

List of Abbreviations			
ALP	alkaline phosphatase	DAT	decellularised adipose tissue
AR	alizarin red	DMEM	Dulbecco's modified Eagle's medium
AT	adipose tissue	ECM	extracellular matrix
ATMP	advanced therapy medicinal products	FBS	foetal bovine serum
BGLAP	bone gamma-carboxyglutamate protein	GAPDH	glyceraldehyde 3-phosphate dehydrogenase
BGP	beta-glycerolphosphate	hDAT	human decellularised AT
CD	cluster of differentiation	hDPSC	human dental pulp stem cell
Col	collagen type I	IBMX	3-isobutyl-1-methylxanthine
DAPI	4',6-diamino-2-phenylindol	IF	immunofluorescence
		LPL	lipoprotein lipase
		MBL	marginal bone loss
		MSC	mesenchymal stem cell

PBS	phosphate buffered saline
PDL	periodontal ligament
pDAT	porcine decellularised AT
PDL	periodontal ligament
PEG	polyethylene glycol
PFA	paraformaldehyde
RPS18	ribosomal protein S18
Q-TOF	quadrupole time of flight
RT-qPCR	reverse transcription quantitative real-time polymerase chain reaction
SEM	scanning electron microscopy
SPARC	secreted protein acidic and cysteine rich
TEM	transmission electron microscopy
UHPLC	ultra-high performance liquid chromatography

Introduction

Bone tissue engineering and regeneration has traditionally received extraordinary attention in some clinical disciplines such as traumatology, orthopaedics and dentistry. In traumatology and orthopaedics, the healing of bone-associated fibrous tissues such as tendons and ligaments represents a major challenge, especially for what concerns the restoration of joint function and mobility (Zhao *et al.*, 2021). In restorative dentistry, the main complication of current dental implants is that they exert an excessive mechanical load on the surrounding alveolar bone in the long term because the pressure exerted on the implant root during mastication is directly transferred to the bone tissue, leading to bone loss and peri-implantitis (Bertolini *et al.*, 2019). In natural teeth, a bone-protective cushioning effect is accomplished thanks to the presence of the PDL, a relatively narrow strip of non-calcified and highly vascularised and innervated connective tissue. Acting as a shock-absorber, the PDL greatly limits the amount of mechanical damage to the alveolar bone during mastication.

One possibility for enhancing the regeneration of bone-associated fibrous ligament tissues could be to inject ECM-derived biomaterials (Nakamura *et al.*, 2019; Zhao *et al.*, 2021). Collagen-containing ECMs are abundant in many body tissues and tissue decellularisation is an excellent approach to isolate these fibrous components. Moreover, thanks to modern 3D bioprinting technologies, these decellularised ECM-derived materials can be used to produce bioinks for personalised tissue engineering (Dzobo *et al.*, 2019; Kabirian and Mozafari, 2020). In this context, an ideal ligament-tissue mimic should have the ability not only to mineralise at the edges for anchoring to calcified tissues but also to harbour blood vessels and nerves in other areas that would remain non-calcified. Such a material should also be able to promote a strong cellular adhesion and an efficient migration/colonisation by MSCs as well as their on-site vascular and osteogenic differentiation,

which are known to be two functionally related processes (Diomedede *et al.*, 2020; Ge *et al.*, 2018; Huang and Li, 2008).

hDPSCs are regarded as some of the most promising stem cells for regenerative dentistry and medicine. These cells can be induced to differentiate towards most of the cell lineages that are naturally present in the oral cavity, including fibroblast, bone cells, vascular cells and even neural cells (Aurrekoetxea *et al.*, 2015; Gronthos *et al.*, 2000; Luzuriaga *et al.*, 2019a; Uribe-Etxebarria *et al.*, 2017). Compared to other oral MSC sources, including those derived from the PDL, hDPSCs are available in larger amounts and better aseptic conditions following tooth extraction (Luzuriaga *et al.*, 2021). hDPSCs can differentiate into bone cells and generate calcified compact bone tissue *in vivo*, as observed both in animal models and human patients (Chamieh *et al.*, 2016; Giuliani *et al.*, 2013). In the clinical context of bone regeneration, the hDPSC source could even be the patients themselves (autologous cell transplant) in a variety of scenarios. Even though hDPSCs in suspension have demonstrated the ability to differentiate into osteoblasts and regenerate relatively small areas of mandibular and alveolar bone (d'Aquino *et al.*, 2009; Giuliani *et al.*, 2013; La Noce *et al.*, 2014), their combination with biomimetic and/or bioactive 3D scaffolds could substantially enhance their effectiveness in healing large bone lesions with or without affecting the temporomandibular joint, such as in cases of serious oral trauma lesions involving the loss of several tooth pieces and relatively large areas of bone tissue.

White AT is highly vascularised, containing large amounts of small- and medium-calibre blood vessels. The ECM of white AT contains collagen fibres (types I and III) and is also rich in basement-membrane proteins such as collagen type IV, laminin and perlecan (sulphated proteoglycan). DAT constitutes one of the most promising biomaterials for tissue engineering due to its easy accessibility, malleability and bioactive properties (Yang *et al.*, 2020). Moreover, it has shown *in vivo* biocompatibility (Wang *et al.*, 2013), opening the door to a yet untapped resource in the context of bone and ligament regeneration. Biological scaffold materials obtained from DATs are known to facilitate the adhesion and functional integration of the seeded cells within the scaffold structure (Yang *et al.*, 2020). A new methodology for AT decellularisation has recently been patented (Web ref. 1). Importantly, DAT can be processed through a large variety of technologies to obtain biological scaffold materials customised for different applications. In the context of bone-tissue regeneration and functional integration, one of the most promising DAT biological scaffold is solid foam, because of its relatively high volume per weight ratio and substantial porosity, thus allowing for a fast mobility of cells, nutrients and signals.

In the present study, hDPSCs were combined *in vitro* with porcine and human DAT (pDAT and hDAT)

solid foams to investigate the effect of these inductive microenvironments on the osteogenesis of hDPSCs in 3D culture. The compatibility and interactions between osteogenic hDPSCs and these new pDAT and hDAT scaffolds was assessed in detail, comparing them to single-protein-based scaffolds of Col, which have already been extensively used in bone tissue engineering applications (Chamieh *et al.*, 2016; Rico-Llanos *et al.*, 2021; Zhang *et al.*, 2018).

Materials and Methods

Porcine and human adipose tissue decellularisation

Human AT was obtained from Biopredict International (permission AC-2013-1754, Saint-Grégoire, France) and porcine AT from a local food company (Jaucha SL, Navarra, Spain). Both tissues were in part stored at -20°C in part processed. Before decellularisation, the tissues were maintained at room temperature for defrosting, cleaned and creamed using a beater. Afterwards, tissues were homogenised on ice using a Polytron[®] PT3100 (Kinematica AG, Malters, Switzerland) with two different rods at 12,000 rpm for 5 min. The homogenised tissue was centrifuged at $900 \times g$ for 5 min after addition of 25 mL ultrapure water to favour the phase separation of lipids, which were discarded manually, keeping the protein pellet accumulated at the bottom of the container during the centrifugation. The pellets were treated with 30 mL pure isopropanol (59307, Merck Life Science) overnight under orbital shaking at 100 rpm at room temperature. Afterwards, the materials were thoroughly cleaned using PBS supplemented with 1 % antibiotic-antimycotics (15240062, Gibco) and 125 μL protease inhibitors (539128, Merck Life Science) and treated with 1 % (v/v) Triton X-100 and 0.1 % (v/v) ammonium hydroxide (221228, Merck Life Science) for 36 h in an orbital shaker 100 rpm at room temperature. Then, the materials were thoroughly cleaned, as previously described, and lyophilised until completely dry. To create a fine-grained powder suitable for processing, the DATs were milled using a mixer mill (Retsch MM400, Biometa Tecnologia y Sistemas, Parque Tecnológico de Asturias, Spain), preceded by freezing in liquid nitrogen, and kept at 4°C in a vacuum desiccator.

Analysis of porcine and human DATs

Remnant DNA and lipids were measured in milled DATs following a previously described methodology (Cicuéndez *et al.*, 2021). Briefly, single and double strain DNA was extracted from the DATs (QiAmp kit, Qiagen) and absolute quantification of DNA content was measured based on a standard curve obtained by serial dilutions of known DNA concentrations to relate the crossing-points (C_p) values of different porcine and human genes. Data are shown as remnant DNA (ng) for dry weight pDAT/hDAT (mg). The detection limit of the technique was estimated in approximately 20 pg. DNA quantification was carried out by DNADATA (San Sebastian, Spain), a Basque

Country Government authorised company for the diagnostic of genetic diseases.

For AT decellularisation, an effective delipidation is also necessary. Chromatography coupled with Q-TOF mass spectrometry (UHPLC/Q-TOF MS) was used to quantitatively analyse the total remnant lipid content in the DAT materials. Briefly, the extracts were injected into a Waters[™] UPLC column ($1.8 \mu\text{m} \times 100 \text{ mm} \times 2.1 \text{ mm}$; Acquity UPLC HSS T3, Waters, Milford, MA, USA) and heated to 65°C . The mobile phases consisted of acetonitrile and water containing 10 mmol/L ammonium acetate (40:60, v/v) (phase A) and acetonitrile and isopropanol containing 10 mmol/L ammonium acetate (10:90, v/v) (phase B). The flow rate was 0.5 mL/min and the injection volume was 5 μL . UHPLC mass spectrometry data were acquired using a SYNAPT G2 HDMS (Waters), with Q-TOF configuration and equipped with an electrospray ionisation source. The mass spectrometry analysis was performed at the Lipidomic Core Facility-SGIKER, University of the Basque Country, Leioa, Spain.

Decellularised porcine and human adipose tissue processing as solid foams

Solid foams of pDAT and hDAT were prepared by the freeze-drying method. 0.5 % (w/v) milled pDAT and hDAT were added to a 0.5 mol/L acetic acid solution and homogenised by magnetic stirring for 48 h at room temperature. After that, different moulds were used to prepare solid foams. For SEM as well as mechanical and swelling testing, 20 mm in diameter and 3 mm in thickness Teflon[™] moulds were used with a 1 mL of solution. For *in vitro* cell culture assays, pDAT and hDAT solutions (approximately 200 $\mu\text{L}/\text{cm}^2$) were added to conventional 48- and 24-well polystyrene tissue culture treated plates or to Millicell EZ-slide 8-well glass slides (PEZGS0816; Merck Millipore), resulting in a 3D cell-culture slide compatible with optical and confocal microscopy. All the samples were frozen at -20°C overnight and freeze-dried (63 Pa and -10°C) for 72 h to obtain the solid foams. For cell culture assays, solid foams were sterilised using ethylene oxide (Esterilizacion SI, Barcelona, Spain).

SEM

Solid foam microarchitecture and porosity was assessed by SEM. The freeze-dried samples were mounted, pulse-coated using a JFC-1100 ion-sputter (JEOL, Tokyo, Japan) with gold (5-10 nm) and visualised using a JEOL JSM-5910 LV SEM (JEOL, Tokyo, Japan) with an accelerating voltage of 10 kV.

Mechanical test

Mechanical properties of the pDAT and hDAT hydrated solid foams were measured by oscillatory shear rheology. Rheological experiments were carried out using a parallel-plate geometry (200 mm diameter steel with a gap of 1 mm) of a Thermo Haake Rheostress RS6000 rheometer (Thermo Scientific). Firstly, stress amplitude sweeps were

performed at a constant frequency of 0.1 Hz to fix the amplitude parameter for each sample and to ensure that subsequent data were collected in the linear viscoelastic regime. All the measurements were made in duplicate at room temperature in constant deformation control mode over a frequency range from 0.01 to 10 Hz.

Swelling properties

Solid foam absorption capability was determined by equilibrium swelling measurements ($n = 5$). The dry weight (W_d) was recorded for lyophilised foams prior to bringing them to maximum hydration in distilled water for 24 h. Thereafter, the foams were carefully blotted to remove the excess liquid and the wet weight (W_s) was recorded. Mass swelling ratio (S) and equilibrium water content (%ECW) were determined using the following equations:

$$S = \frac{W_s - W_d}{W_d}$$

$$\%ECW = \frac{W_s - W_d}{W_s} \times 100$$

hDPSC culture

Primary cultures of hDPSCs from third molar teeth were established following a well-established protocol (Irastorza *et al.*, 2019; Uribe-Etxebarria *et al.*, 2020). Briefly, healthy young (age 18-40) patients who had been prescribed a tooth extraction for external reasons inherent to their clinical care process were recruited from dental clinics, where they gave their informed consent for tooth donation. This protocol received the approval of the CEISH committee of UPV/EHU for research with human samples and abided by the ethical principles of the Declaration of Helsinki on medical research involving human subjects. The collected teeth were fractured and enzymatic digestion of the pulp tissue was carried out for 1 h at 37 °C using 3 mg/mL collagenase (17018-029, Thermo Fisher Scientific) and 4 mg/mL dispase (17105-041, Thermo Fisher Scientific), followed by mechanical dissociation. Then, DPSCs were cultured in DMEM supplemented with 10 % FBS, 1 mmol/L L-glutamine and the antibiotics penicillin (100 U/mL) and streptomycin (150 µg/mL). Under these conditions, hDPSCs typically acquire an MSC-like phenotype characterised by the expression of nestin, CD90, CD73 and CD105 (Irastorza *et al.*, 2019; Luzuriaga *et al.*, 2019b). After the first culture passage, 15,000-50,000 cells were transferred to cell culture plates and/or customised 8-well Minicell EZ-slides where some wells were filled with a layer of equal volume of solid foam pDAT, hDAT and Col bioscaffolds for 3D culture, whereas others were left empty with their original 2D design as control.

Osteogenic and adipogenic differentiation of hDPSCs

In all experiments, hDPSCs were cultured in parallel in solid-foam-filled and control empty wells. Moreover, hDPSCs under both these conditions were

also cultured with or without osteogenic medium for osteodifferentiation. The osteogenic differentiation medium consisted of DMEM supplemented with 50 µmol/L ascorbic acid (A4403, Sigma-Aldrich), 20 mmol/L β-glycerolphosphate (50020, Sigma-Aldrich) and 10 nmol/L dexamethasone (D4902, Sigma-Aldrich). Cells were cultured for varying times between 2 and 4 weeks for different experiments. For some experiments, hDPSCs were also cultured with adipogenic differentiation medium, consisting of 0.5 mmol/L IBMX (I5879, Sigma-Aldrich), 1 µg/mL insulin (91077C, SAFC Biosciences, St. Louis, MO, USA) and 1 µmol/L dexamethasone for 4 weeks.

ALP staining

After culturing hDPSCs for 14 d in hDAT, pDAT and collagen, samples were fixed briefly using 4 % PFA for 1 min and washed with 0.05 % Tween 20-PBS. ALP staining was performed using 5-bromo-4-chloro-3-indolyl phosphate/nitro blue tetrazolium (B3804, Sigma-Aldrich) as a substrate and the staining progress was checked every 3 min. After incubation, the cells were washed with PBS three times for 5 min. The images were acquired using a stereoscopic microscope Zeiss Stemi 2000-C and a Canon PowerShot A80 camera. ALP absorbance in EZ-slides was semi-quantitatively analysed using Image J software (NIH), by measuring average pixel intensity in the green image channel after background subtraction. ALP absorbance in 24- and 48-well plates was measured at 420 nm using a Synergy HT Multi-Mode Microplate Reader (Biotek, Winooski, VT, USA). Microscopy images were obtained using a stereoscopic microscope Zeiss Stemi 2000-C and Canon PowerShot A80 camera.

AR staining

hDPSCs cultured for 4 weeks in hDAT, pDAT and collagen solid foams were fixed using 4 % PFA for 10 min. Samples were washed with distilled water and stained using 2 % AR (Acros Organic, Sigma-Aldrich) at pH 4.1-4.3 for 45 min in the dark at room temperature. The staining solution was removed and samples were washed with distilled water until no AR could be seen dissolved in the water. The images of stained calcified bone-tissue matrix areas were acquired using a stereoscopic microscope Zeiss Stemi 2000-C and a Canon PowerShot A80 camera. AR absorbance in EZ-slides was semi-quantitatively analysed using Image J software, by measuring average pixel intensity in the green image channel after background subtraction. AR absorbance in 24- and 48-well plates was measured at 405 nm using a Synergy HT Multi-Mode Microplate Reader (Biotek). Thereafter, foams were detached from culture plates and mounted onto microscopy slides to obtain higher resolution images. Cell nuclei were counterstained using DAPI (1:1000; Invitrogen). Images of mounted foams were acquired using an epifluorescence and transmitted light Olympus IX71 microscope, coupled to an Olympus DP71 digital camera.

Table 1. List of the sequences of primers used in this study. Tm: melting temperature in °C. F: forward. R: reverse.

Primers		Sequence 5'-3'	Tm	Lenght	Amplicon size (bp)
LPL	F	ACACAGAGGTAGATATTGGAG	53.88	21	143
	R	CTTTTCTGAGTCTCTCCTG	52.98	22	
ALPL	F	TCTTCACATTTGGTGGATAC	52.89	20	154
	R	ATGGAGACATTCTCTCGTTC	54.6	20	
B-ACTIN	F	GTTGTCGACGACGAGCG	58.55	17	93
	R	GCACAGAGCCTCGCCTT	59.68	17	
RPS18	F	CAGAAGGATGTAAAGGATGG	53.05	20	200
	R	TATTTCTTCTTGGACACACC	52.82	20	
GAPDH	F	CTTTTGCGTCGCCAG	52.78	15	139
	R	TTGATGGCAACAATATCCAC	53.92	20	

Oil red O staining

hDPSCs were cultured for 4 weeks in hDAT, pDAT and collagen solid foams. Then, samples were fixed using 4 % PFA for 10 min and stained with a 0.5 % oil red O (O-0625, Sigma-Aldrich) solution in PEG for 15 min. After staining, foams were washed with a 60 % PEG solution and 2 times with distilled water for 1 min. Cell nuclei were counterstained with DAPI (1:1000; Invitrogen) in PBS. Thereafter, foams were detached from the culture plates and mounted onto microscopy slides to obtain higher resolution images. Images of mounted foams were acquired using an epifluorescence and transmission light Olympus IX71 microscope, coupled to an Olympus DP71 digital camera.

RNA extraction and RT-qPCR

RNA was extracted from the solid foams by adding a solution of TRIzol (10296010, Ambion) and chloroform (C0549-1PT, Sigma-Aldrich) at a 4:1 ratio. Foams were readily dissolved in this solution by gentle pipetting. Then, the samples were transferred into ultracentrifuge tubes and centrifuged for 15 min at 12,000 ×g and 4 °C to obtain organic and aqueous phases. The upper aqueous phases were collected and RNA was precipitated by adding an equal volume of isopropanol. The solution was incubated for 10 min. Thereafter, then samples were centrifuged again for 10 min at 12,000 ×g and 4 °C, when precipitated RNA formed a gel-like pellet that was washed with a 75 % ethanol solution and resuspended in 20 µL of elution buffer (12183020, Invitrogen RNA mini kit). RNA purity and concentration were calculated using a spectrophotometer Synergy HT (Winooski, VT, USA) at 260/280 nm. Reverse transcription reaction was performed using iScript™ cDNA synthesis Kit (BioRad). RT-qPCR experiments were conducted using an iCycler My iQ™ Single-Color Real-Time PCR Detection System (BioRad), using 4.5 µL of Power SYBR® Green PCR Master Mix 2× (4367659, Applied Biosystems™), 0.5 µL of primers (0.3125 µmol/L), 0.3 µL of cDNA (1.5 ng/µL) and nuclease-free water for a total volume reaction of 10 µL. All primers were obtained from public databases and checked for optimal efficiency (> 90 %) under the study RT-qPCR experimental conditions.

RT-qPCR was performed using a CFX96® thermo cycler (BioRad). Data were processed using the CFX Manager™ Software (BioRad). All RT-qPCR reactions yielded only one amplicon as assessed by the melting curve method. The sequences of primers are listed in Table 1.

IF

After culturing hDPSCs for 14 d onto hDAT, pDAT and collagen solid foams, cells were washed with PBS and fixed using 4 % PFA for 10 min at room temperature. Next, cells were incubated with 10 % goat serum (50197Z, Invitrogen) for 10 min at room temperature. Then, the following primary antibodies were applied at a dilution of 1:200 overnight at 4 °C in a solution of 0.1 % Triton X-100 and 1 % BSA in PBS: rabbit anti-osteocalcin/BGLAP (ab93876, Abcam), rabbit anti-osteonectin/SPARC (ab14174, Abcam). Thereafter, secondary antibody goat anti-rabbit Alexa Fluor™ 488 (1:200, A32731, ThermoFisher Scientific) was applied for 1 h at room temperature. Cell nuclei were counterstained with DAPI (1:1000; Invitrogen). Images were acquired using a confocal microscope Zeiss LSM800 (Zeiss) coupled to an Axiocam 305 (Zeiss) colour camera. Relative IF intensity in images taken from EZ-slides was calculated by dividing the overall IF labelling by the number of nuclei present in the confocal plane. Quantification of BGALP intensity in solid foams incorporated into cell culture plates was performed by fluorimetry (excitation 480 nm; emission 525 nm) using a Synergy HT Multi-Mode Microplate Reader (Biotek).

TEM

After 15 min fixation in 2 % glutaraldehyde (in 0.1 mol/L Sörenson phosphate buffer, pH 7.2), samples were embedded in Epon Polarbed 812 resin (Electron Microscopy Sciences, Hatfield, PA, USA). Ultrathin sections (70 nm; Leica UCT ultramicrotome) were deposited onto 150 mesh copper grids (G2150C, 150 Square Mesh copper 3.05 mm, AGAR Scientific, Essex, UK), post-stained with 2 % uranyl acetate in distilled water (AGR1260A, AGAR Scientific) and 0.2 % lead citrate in distilled water (AGR1210, AGAR Scientific), and visualised using a sCMOS Hamamatsu digital camera (Hamamatsu, Japan).

Statistical analysis

The experimental data were statistically analysed using SPSS version 26 (IBM). All data sets were subjected to a normality test to verify whether they fitted or not to a normal distribution. Statistical comparisons between sample groups were then made by either parametric or non-parametric tests: Student's *t*-test (only 2 samples) and/or ANOVA with Tukey's *post-hoc* test (multiple samples) for normal distributions; Mann Whitney U-test (2 samples) and/or Kruskal-Wallis with Dunn's *post-hoc* test (multiple samples) for distributions that did not meet normality criteria. Confidence intervals were set at 95 % ($p < 0.05$), 99 % ($p < 0.01$) and 99.9 % ($p < 0.001$).

Results

Characterisation of human and porcine decellularised ATs and solid foams

Based on previous experience in effective AT decellularisation (Cicuéndez *et al.*, 2021; Web ref. 1), in the present study porcine and human ATs were decellularised by following the organic solvent method previously developed in house and based on a modified published methodology (Brown *et al.*, 2011). Specifically, the method used isopropanol and a non-ionic detergent such as Triton X-100 and,

as previously reported (Cicuéndez *et al.*, 2021), the resultant pDAT and hDAT materials met the decellularisation criteria established by the research community and standard guides (Crapo *et al.*, 2011; Web ref 2). Briefly, this processing method produced biomaterials with a remnant DNA of 3.71 ± 1.2 and 24.8 ± 2.05 ng/mg for hDAT and pDAT, respectively. Effective lipid removal is essential for AT decellularisation, so pDAT and hDAT remnant lipids were also quantified. pDAT showed a maximum of 7.0 ± 0.2 % (w/w) remnant total lipids (69.6 ± 2.1 µg/mg) and hDAT of 0.6 ± 0.2 % (w/w) (5.8 ± 1.5 µg/mg). Concerning the types of lipids analysed, both hDAT and pDAT remnant lipids were mostly triacylglycerols. Finally, the most of native ECM and basement membrane proteins are conserved in both pDAT and hDAT materials (Cicuéndez *et al.*, 2021).

Once the decellularisation criteria were verified, pDAT and hDAT materials were processed as solid foams when used as biological scaffolds for 3D cell cultures *in vitro* (Fig. 1a,b). Milled pDAT and hDAT materials were optimally processed to obtain solid foams by the freeze-drying method and SEM analysis revealed a highly interconnected porous mesh-like structure, with a pore size of 50-100 µm (Fig. 1c,d). Solid foams swelled properly without losing their geometry and showed excellent swelling values. The two solid foams slightly differed in their water-

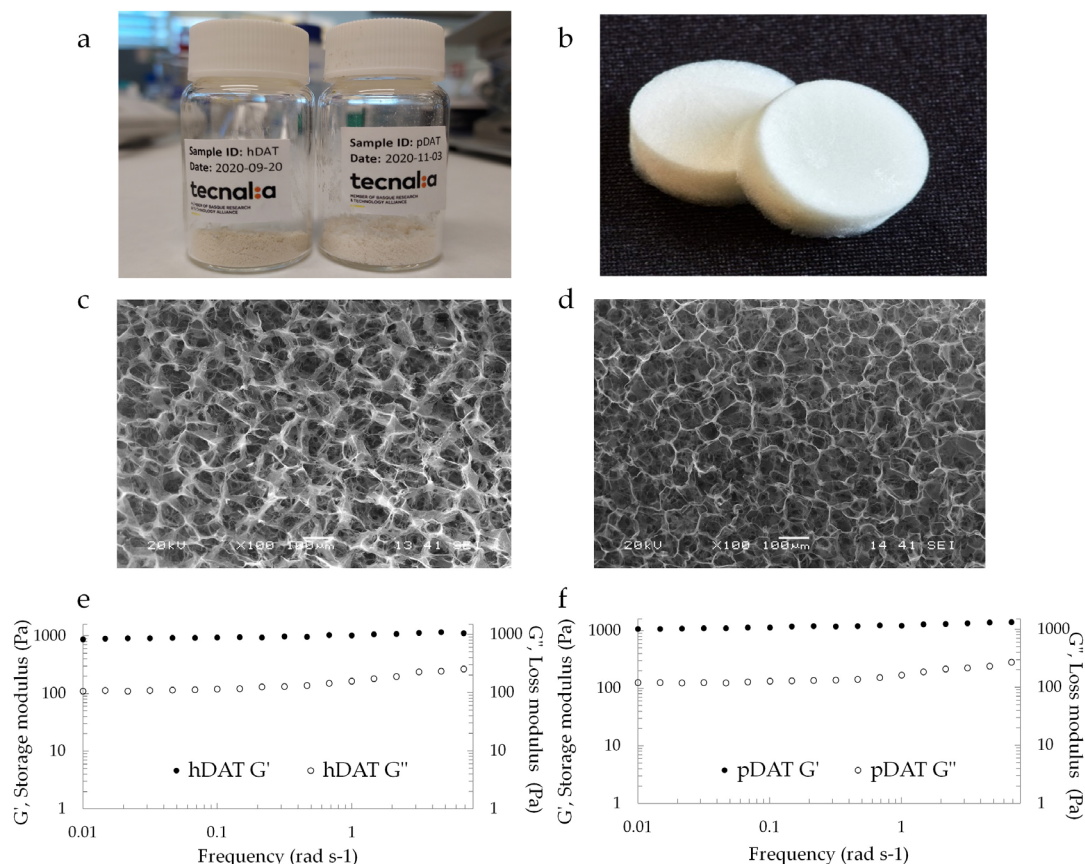


Fig. 1. Decellularisation of AT and characterisation of pDAT and hDAT processed as solid foam by freeze-drying. (a) Powder form of pDAT and hDAT prepared for processing. (b) Dried solid foam. (c,d) SEM images of solid foams showing the highly interconnected pore microstructures (scale bar: 100 µm) in (c) hDAT and (d) pDAT. (e,f) Rheological behaviour of solid foams showing storage (G') and loss modulus (G'') over a frequency from 0.01 to 10 Hz: (e) hDAT and (f) pDAT.

retaining abilities. pDAT solid foams showed higher values ($S=76.1\pm 8.1$ and $ECW=98.7\pm 0.1\%$) than hDAT solid foams ($S=32.8\pm 1.9$ and $ECW=97.0\pm 0.2\%$). The viscoelastic behaviour of the solid foams was measured by oscillatory shear rheology at the selected amplitude of 0.02 Pa and scanning the frequency (0.01-10 rad/s) at this constant amplitude (Fig. 1e,f). The solid foams showed higher G' (storage modulus) than G'' (loss modulus) values over the entire range of frequencies, indicating the predominance of the elastic behaviour over the viscous one. The solid foams exhibited a young modulus of $1,194.7\pm 106.7$ Pa and 990.25 ± 91.8 Pa for pDAT and hDAT, respectively.

Culture of hDPSCs on solid foams

The solid foam scaffolds were integrated with either 8-well Minicell EZ slides (PEZGS0816, Merck Millipore) or in conventional 24- and 48-well cell culture plates to generate customised lid-covered 3D tissue culture devices where hDPSCs were seeded at 15,000-50,000 cells/well, depending on the well size. In the presence of 10 % FBS, hDPSCs tend to naturally differentiate towards osteoblast-like cells (Pisciotta *et al.*, 2012). The study hypothesis was that the intricate porous structure of 3D solid foams would generate ideal conditions for the deposition of the newly formed osteoid matrix over the collagen

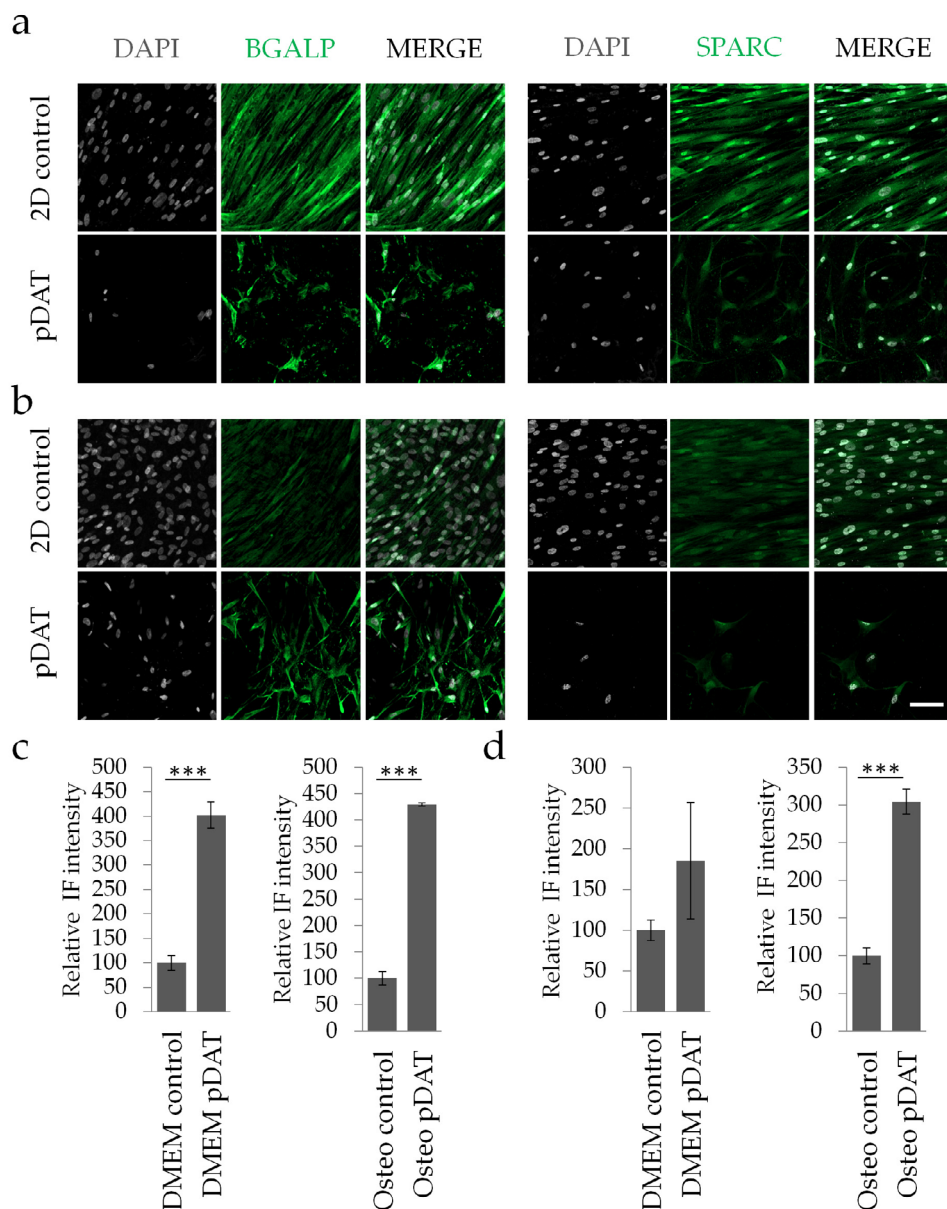


Fig. 2. Expression of osteocalcin/BGLAP and osteonectin/SPARC by hDPSCs seeded onto 3D pDAT solid foams. hDPSCs were seeded on either empty (plastic bottom) or pDAT-containing EZ-slide wells and cultured in parallel for 2 weeks, in both control (DMEM 10 % FBS; DMEM) and osteodifferentiation enhancement conditions (DMEM 10 % FBS + dexamethasone, BGP, ascorbic acid; Osteo). The expression of BGLAP and SPARC was assessed by IF. (a) hDPSCs in control conditions. (b) hDPSCs in Osteo conditions. Scale bar: 50 μ m. (c) Quantification of the relative BGLAP IF labelling relative to cell number, in DMEM and Osteo conditions. (d) Quantification of relative SPARC labelling in DMEM and Osteo conditions. $n = 3-5$, *** $p < 0.001$, Student's t -test.

fibres present in the pDAT and hDAT. To compare osteogenic differentiation in 3D with respect to control 2D plastic-adherent culture conditions, hDPSCs were grown in parallel in empty *vs.* pDAT-filled wells within the EZ slides (Fig. 2). Experimental conditions of enhancement of the osteoblastic differentiation process of hDPSCs were also included, and to this end, another well-established protocol was employed, namely the addition of dexamethasone, β -glycerophosphate and ascorbic acid (Langenbach and Handschel, 2013). Cell cultures were allowed to grow in EZ slides for 2 to 4 weeks. DAPI staining showed a good viability of hDPSC cultures at all time points, with a near total absence of pyknotic nuclei. hDPSCs migrated and were distributed through the 3D scaffolds and could be located at different focal planes at the end of the culture period. Thus, the cellular density on single confocal planes within 3D cultures was lower than at the bottom of control 2D

wells, where all the hDPSCs concentrated on a single plane and readily formed confluent surface-adherent cell monolayers (Fig. 2a,b).

hDPSCs cultured on solid foams expressed markers of bone-producing osteoblastic cells

After 14 d of cell culture on either EZ slide plastic surfaces or pDAT solid foams, the expression of osteoblastic differentiation markers was examined by IF. The extracellular bone matrix proteins osteocalcin/BGLAP and osteonectin/SPARC were chosen as most representative of osteoblastic cell commitment (Jeon *et al.*, 2018; Sommer *et al.*, 1996). hDPSCs grown in both plastic surfaces and pDAT solid foams expressed detectable amounts of BGLAP and SPARC. The average IF relative intensity was almost always higher in pDAT-grown cells, both under control and osteogenic differentiation conditions ($p < 0.001$, Student's *t*-test; Fig. 2c). In cells grown under plastic-

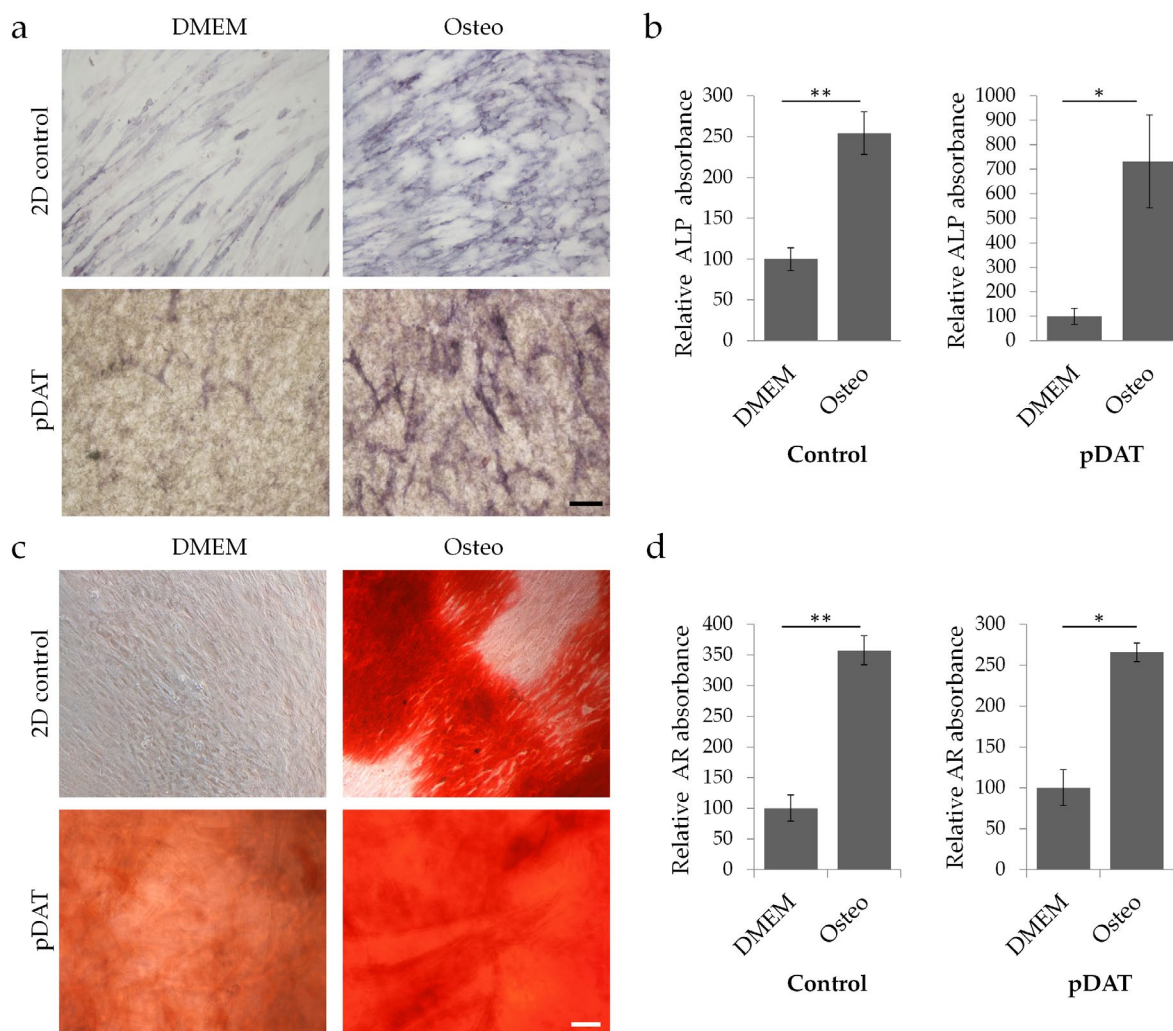


Fig. 3. Detection of ALP activity and calcified bone ECM production by hDPSCs seeded onto pDAT solid foams. hDPSCs were seeded onto either empty (plastic bottom) or pDAT-containing EZ-slide wells and cultured in parallel, in both control (DMEM) and osteodifferentiation enhancement conditions (Osteo). (a) ALP activity was detected by the formation of purple colour precipitates after 2 weeks. Scale bar: 100 μ m. (b) Quantification of the relative ALP absorbance in plastic and pDAT-containing wells in control and Osteo conditions. (c) Calcified bone matrix deposition was detected by AR staining after 4 weeks. Scale bar: 100 μ m. (d) Quantification of the relative AR absorbance in empty and pDAT-containing wells, in DMEM and Osteo conditions. $n = 3$, * $p < 0.05$, ** $p < 0.01$, Mann Whitney's U test.

adherent conditions, a different SPARC localisation could be observed: about $\frac{2}{3}$ of hDPSCs showed a nuclear expression for this protein, whereas the rest showed a predominantly cytoplasmic staining (Fig. 2a,b). In contrast, hDPSCs grown on pDAT solid foams showed predominantly a cytoplasmic/extracellular staining for SPARC, with a less prominent nuclear staining.

hDPSCs cultured on solid foam pDAT upregulated ALP activity and enhanced the deposition of mineralised bone matrix after osteoinduction

To corroborate that hDPSCs were differentiating towards osteoblastic cell lineages on pDAT solid foams, an assay for ALP activity, which is another prominent characteristic of mineralising bone cells (Vimalraj, 2020), was performed. After 2 weeks of cell culture, ALP activity could be detected in hDPSCs grown on both 2D surfaces and 3D pDAT solid foams (Fig. 3a). This ALP activity was significantly

upregulated in cells exposed to osteodifferentiation treatments, both on surface-adherent and pDAT 3D cultures (Fig. 3b). The definite hallmark of complete and mature osteoblastic differentiation is the production of mineralised bone matrix, which can be stained with calcium-binding dyes such as AR (Jeon *et al.*, 2018; Ovchinnikov, 2009). To compare the production of hard calcified bone ECM by hDPSCs, they were cultured in parallel with EZ slide wells, with or without pDAT. After a period of 4 weeks in culture, many of the control wells had a high cell confluence and only occasional AR+ bone matrix precipitates could be observed. In contrast, the presence of mineralised bone-like matrix was much larger in hDPSC cultures subjected to osteodifferentiation (Fig. 3c). In the case of pDAT-grown hDPSC cultures, a better basal mineralising activity was observed using this 3D culture system, in comparison to conventional 2D adherent cultures (Fig. 3c). Again, a strong increase in the AR signal

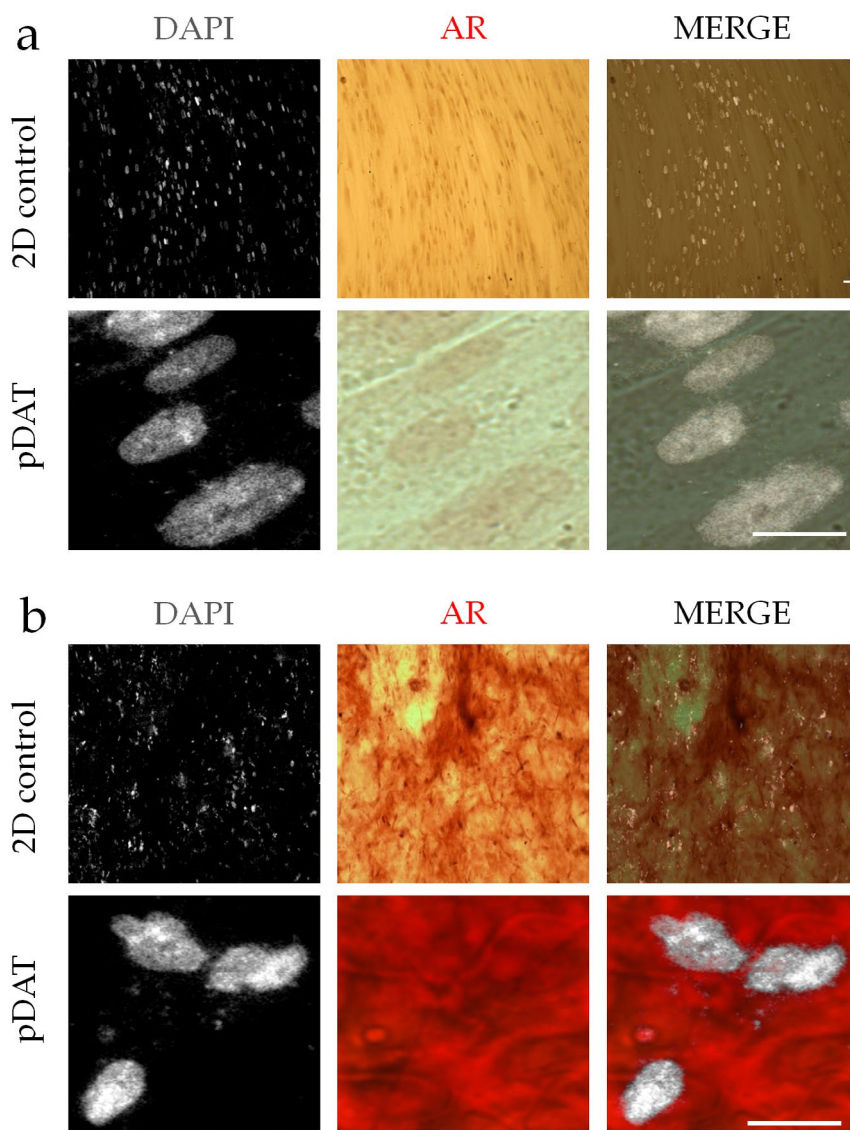


Fig. 4. AR-DAPI double staining showing the localisation of cell nuclei within bone matrix inclusions. hDPSCs were seeded onto (a) either empty or (b) pDAT-containing EZ-slide wells and cultured in parallel for 4 weeks. Samples were double stained with AR and DAPI. Scale bar: (a) 30 μ m; (b) 5 μ m.

was observed when hDPSCs were grown in parallel with pDAT under osteodifferentiation conditions (Fig. 3c,d).

Osteogenic cells in solid foams appeared embedded and in close contact with the AR+ bone matrix precipitates

One inherent characteristic of mature bone cells is that they eventually become completely surrounded by the calcified bone ECM, thus completing their maturation cycle from osteoblasts to osteocytes (Franz-Odenaal *et al.*, 2006). To assess in more detail the interaction of hDPSC-derived cells with the newly produced mineralised matrix, DAPI was included as a counterstain for cellular nuclei and the relative location of cellular bodies was observed with respect to the bone matrix precipitates, by combined bright field and fluorescence microscopy (Fig. 4). Interestingly, some of the cells appeared to be embedded and/or in very close association with the calcified bone matrix. Cell nuclei with a healthy morphology were observed in deep contact with the calcified nodules, supporting a terminal osteocyte differentiation under these conditions.

hDPSCs grown in solid foams mineralised the scaffolds by intramembranous ossification and might differentiate into osteoblasts and adipocytes

To examine more in detail the ultrastructure of the bone-like ECM that was generated by hDPSCs

seeded onto pDAT solid foam scaffolds, TEM analysis was performed. Under control conditions, large areas containing small thin collagen fibres could be observed in the pDAT matrix scaffold, together with some interspersed lipid droplets associated with remains from decellularised AT. Interestingly, sharp transitions between areas containing thin collagen fibres and other areas containing thicker and more mineralised (electron dense) collagen fibres could also be identified (Fig. 5a,6a; yellow dashed lines). These thick and characteristically band-patterned collagen fibre bundles were juxtaposed and apparently connecting to the rest of the pDAT solid foam containing thinner and less calcified collagen. Within the solid foam areas that contained thick electron-dense collagen bundles, intramembranous ossification sites could also be identified (arrowheads in Fig. 6a). Electron-dense areas containing mineralised bone matrix could be found anchored to the rest of the collagen network by Sharpey-like fibres (asterisks in Fig. 6a).

Electron-dense thick collagen fibre bundles and intramembranous ossification sites were more abundant in culture samples subjected to osteodifferentiation induction but were not found in control solid foams without cell seeding, which was indicative that these structures were *de novo* produced by the *in vitro* grown hDPSCs. As expected, some differentiated osteoblastic cells could also be found in the solid foams, associated with matrix

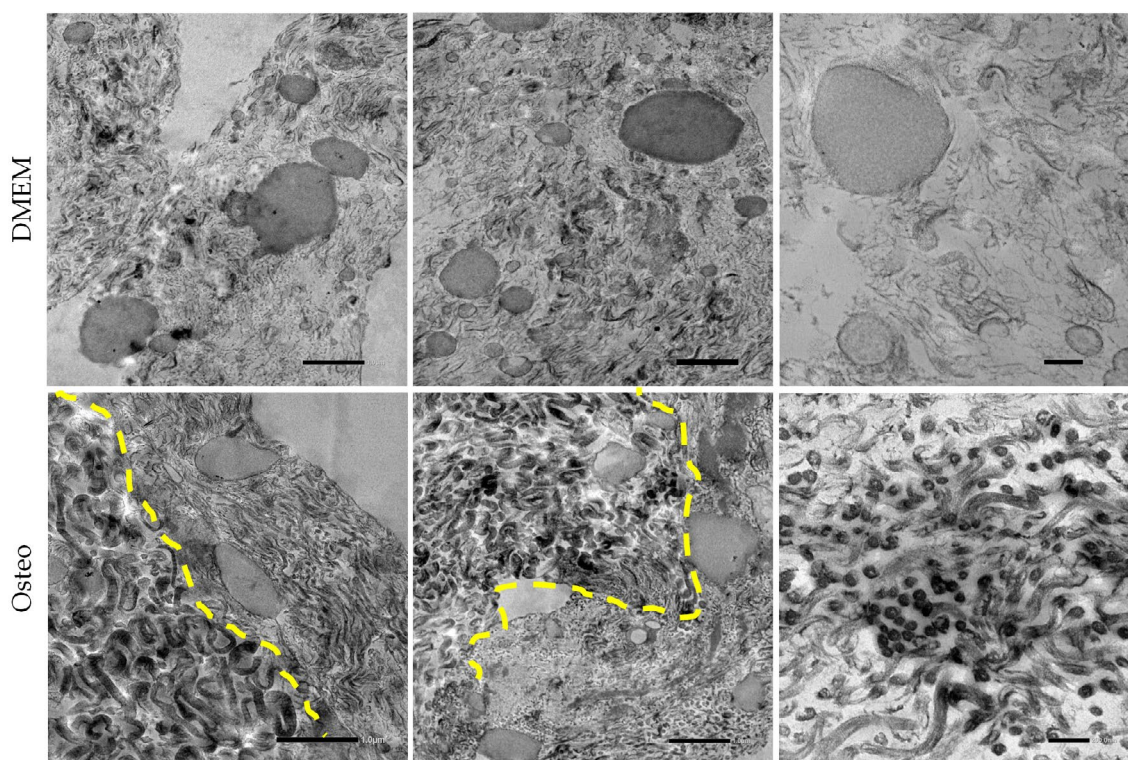


Fig. 5. TEM images showing the ultrastructural features of hDPSC-seeded pDAT solid foams. hDPSCs were grown on pDAT solid foams for 4 weeks, under control (DMEM) and osteodifferentiation enhancement conditions (Osteo). Transition areas between pDAT solid foam matrix containing thinner collagen and hDPSC-generated bone ECM containing thicker and more calcified collagen fibres could be observed (yellow dashed lines). Thick electron-dense collagen fibre bundles were more abundant in osteodifferentiation conditions. Scale bar: 1 μ m (left-hand, and central images), 200 nm (right-hand images).

areas containing thick calcified collagen bundles. These cells had a characteristic mature osteoblastic morphology, showing a rounded cell shape and a secretory phenotype featured by the presence of numerous cytoplasmic vesicles (Fig. 6b). Strikingly, mature multilocular adipocyte-like cells could be detected as well, which were characterised by the presence of numerous intracellular lipid droplets (Fig. 6c). These lipid-storing cells had differentiated from hDPSCs in the pDAT solid foams without the need for addition of any adipogenic differentiation stimulus.

hDAT, pDAT and collagen solid foams showed a differential permissiveness to osteoinduction in 3D hDPSC cultures

A comparative assessment between 2D and 3D cultures is not the ideal scenario to evaluate the possible application of new DAT bioscaffolds in clinical therapy, in comparison with currently available biomaterials. Therefore, single-protein bioscaffolds of Col, the most abundant protein of the bone matrix, were chosen as a positive control for an ECM protein formulation with a proven

capacity to sustain osteogenesis (Rico-Llanos *et al.*, 2021). Similarly, and given that adipose tissue can be extracted from human donors as well, the osteogenic differentiation ability of hDPSC cultures grown in parallel in pDAT and hDAT was compared.

ALP staining was performed, in parallel, on 3D hDPSC cultures in hDAT, pDAT and Col scaffolds. Strikingly, hDAT matrix had a much lower capacity to sustain osteodifferentiation of hDPSCs than the other two scaffolds. Both pDAT and Col showed an important ALP activity 2 weeks after hDPSC seeding, both under control and osteodifferentiation culture conditions. However, only a marginal ALP activity could be detected in hDAT samples (Fig. 7a). A quantitative photometric measurement of ALP absorbance in the samples showed significant differences between hDAT and pDAT/Col under both control and osteodifferentiation conditions ($p < 0.05$, Dunn's *post-hoc*, Kruskal-Wallis; Fig. 7b). RT-qPCR experiments were also performed to assess the expression of *ALP*. Differences between the three bioscaffolds were not evident at the gene expression level in control samples but a significantly higher expression of *ALP* transcript was detected

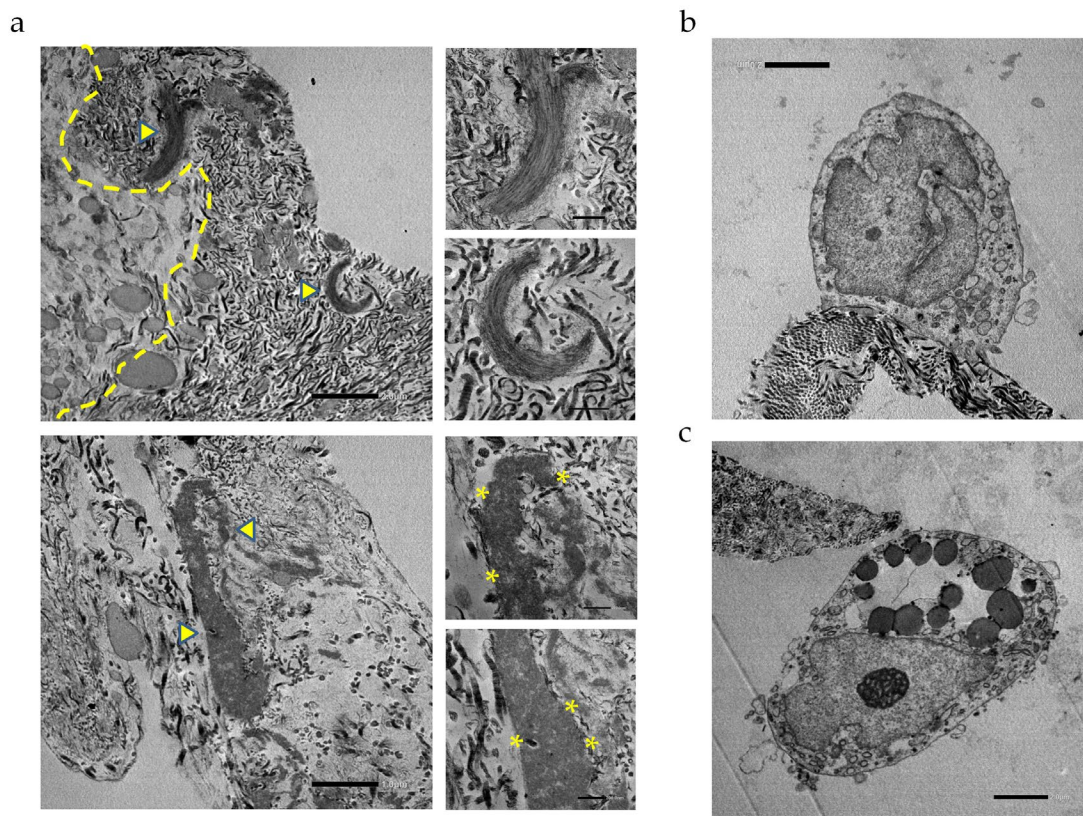


Fig. 6. TEM images showing intramembranous ossification sites and cellular phenotypes obtained on the pDAT solid foams. (a) hDPSC-seeded pDAT solid foams showing the transition between non-calcified thin-collagen areas and calcified thick-collagen fibre bundle areas (dashed-line). Within the thick-collagen-containing areas, some especially electron-dense structures were identified as intramembranous ossification sites. Areas marked by arrowheads are magnified in the right-hand panels. Intramembranous ossification sites showed the presence of perforating Sharpey-like fibres on their edges (asterisks in right-hand panels), which anchored them to the rest of the collagen matrix. Scale bar: 2 μm (left-hand images); 500 nm (right-hand magnified images). (b) Osteoblastic cells were identified on pDAT samples. (c) Multilocular adipocytes were also identified on pDAT samples. Scale bar: 2 μm .

in Col samples with respect to hDAT after 2 weeks in culture under osteodifferentiation conditions ($p < 0.05$, Tukey's *post-hoc* test, one-way ANOVA; Fig. 7c). IF experiments were also performed to detect the presence of osteocalcin/BGLAP in the three solid foams in parallel. A significantly smaller IF intensity of BGLAP was found in hDAT samples with respect to Col ones, as assessed by plate fluorimetry after 2 weeks in culture, in both control and osteodifferentiation conditions (Fig. 8a,b). Interestingly, significant differences were also found in BGLAP IF between pDAT and Col culture samples, with higher IF levels in the latter ($p < 0.05$, Dunn's *post-hoc* test, Kruskal-Wallis).

To determine whether these changes in BGLAP and ALP activity and expression would result in a different mineralising capacity of the hDPSC cultures in each of the three solid foams, AR stainings were performed 4 weeks post-seeding and the absorbance of the 3D culture samples measured at 405 nm (Fig. 9a,b). The three foams tended to absorb some of the staining even in empty samples containing no cells. Thus, it was not possible to detect significant differences between the three scaffolds in control conditions. However, clear differences arose when measuring AR in samples exposed to osteodifferentiation conditions. hDAT bioscaffolds showed a significantly lower tendency

for mineralisation by hDPSCs, in contrast to pDAT and Col ($p < 0.01$, Tukey's *post-hoc* test, one-way ANOVA, Fig. 9b).

A lower osteogenic capacity of hDPSCs on hDAT came at the expense of a higher adipogenic capacity

Given that the TEM analysis had shown that hDPSCs could differentiate not only towards osteoblasts but also towards adipocytes in DAT solid foams, the next question was whether the differences in osteogenic capacity between hDAT and pDAT/Col bioscaffolds could be partly the result of a different adipogenic capacity. To this end, an RT-qPCR analysis of the mature-adipocyte gene marker *LPL* was performed. Interestingly, significantly higher levels of *LPL* expression were found in hDAT-seeded scaffolds, up to about 7 times more with respect to both pDAT and Col ($p < 0.001$, Tukey's *post-hoc* test, one-way ANOVA, Fig. 10a). Those differences were corroborated by performing oil red O staining experiments in hDPSC cultures in hDAT, pDAT and Col scaffolds. To this end, adipogenesis was also compared in control conditions and in the presence of adipogenic induction media. hDPSC cultures in hDAT showed a higher adipogenic capacity, which was particularly evident under control culture conditions, with respect to pDAT/Col ($p < 0.001$, Dunn's *post-hoc* test, Kruskal-Wallis; Fig. 10b). Under

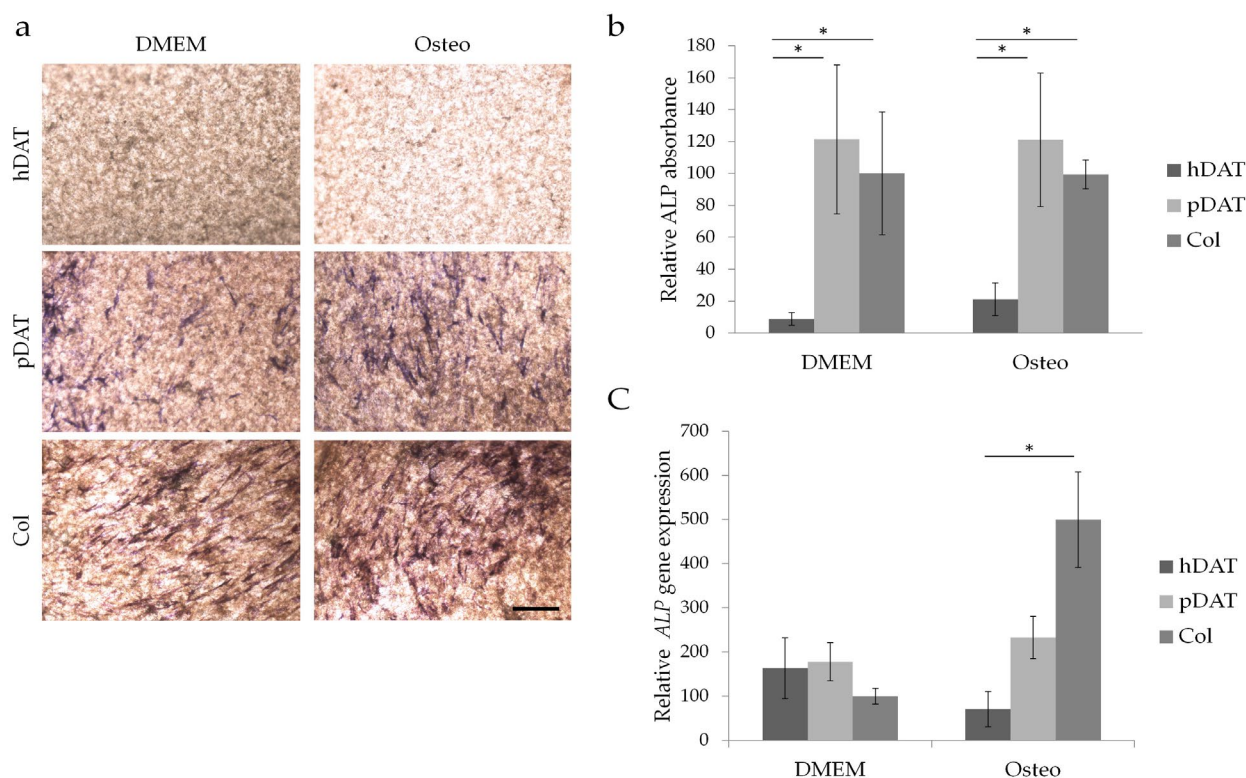


Fig. 7. ALP activity in 3D hDPSC cultures with hDAT, pDAT and Col solid foams. ALP activity and gene expression were assessed after 2 weeks in culture, using the three scaffolds with the same hDPSCs in parallel. (a) Cells showing ALP activity were stained in purple colour within the pDAT and Col foams. Very little ALP activity was detected in hDAT foams, both in control (DMEM) and osteodifferentiation (Osteo) conditions. Scale bar: 500 μ m. (b) Photometric quantification of ALP absorbance at 420 nm, $n = 4-7$, * $p < 0.05$, Dunn's *post-hoc*, Kruskal-Wallis. (c) RT-qPCR analysis of *ALP* expression, $n = 3-6$, * $p < 0.05$, Tukey's *post-hoc* test, one-way ANOVA.

adipogenic induction conditions the differences between scaffolds tended to dilute but the hDPSC cultures on hDAT still showed the highest oil red O levels, with nearly statistically significant differences with respect to pDAT ($p = 0.07$, Dunn's *post-hoc* test, Kruskal-Wallis).

Discussion

The development of innovative 3D culture systems, that allow for a more accurate assessment of the interactions that take place between cells and the ECM in live tissues, remains a priority for regenerative stem-cell-based therapies. Very useful information may be obtained using 3D culture systems before moving to *in vivo* studies and clinical trials (Keller *et al.*, 2006). Thanks to the development of tissue decellularisation technologies, it is nowadays possible to obtain completely ECM-derived materials

from a large variety of tissues. These materials show excellent processability as biological scaffolds that not only provide a substrate for cell attachment but also a plethora of potential bioinductive signals to the seeded cells, which may influence their differentiation outcome (Vasanthan *et al.*, 2021).

Regarding tissue engineering of skeletal and joint structures after traumatic lesions using cell therapy, it is important not only to be able to regenerate the calcified bone tissue but also the associated fibrous connective tissues, such as tendons and ligaments. These connective tissue structures must still undergo some degree of calcification, especially at the edges, to make a solid insertion within mineralised bone tissue, but they must also retain the ability to keep a soft structure to harbour nerves and vasculature. In this case it could be very interesting to apply biomaterials with a different mineralisation capacity, to regenerate different types of affected tissues. Single-protein scaffolds such as Col have been successfully used

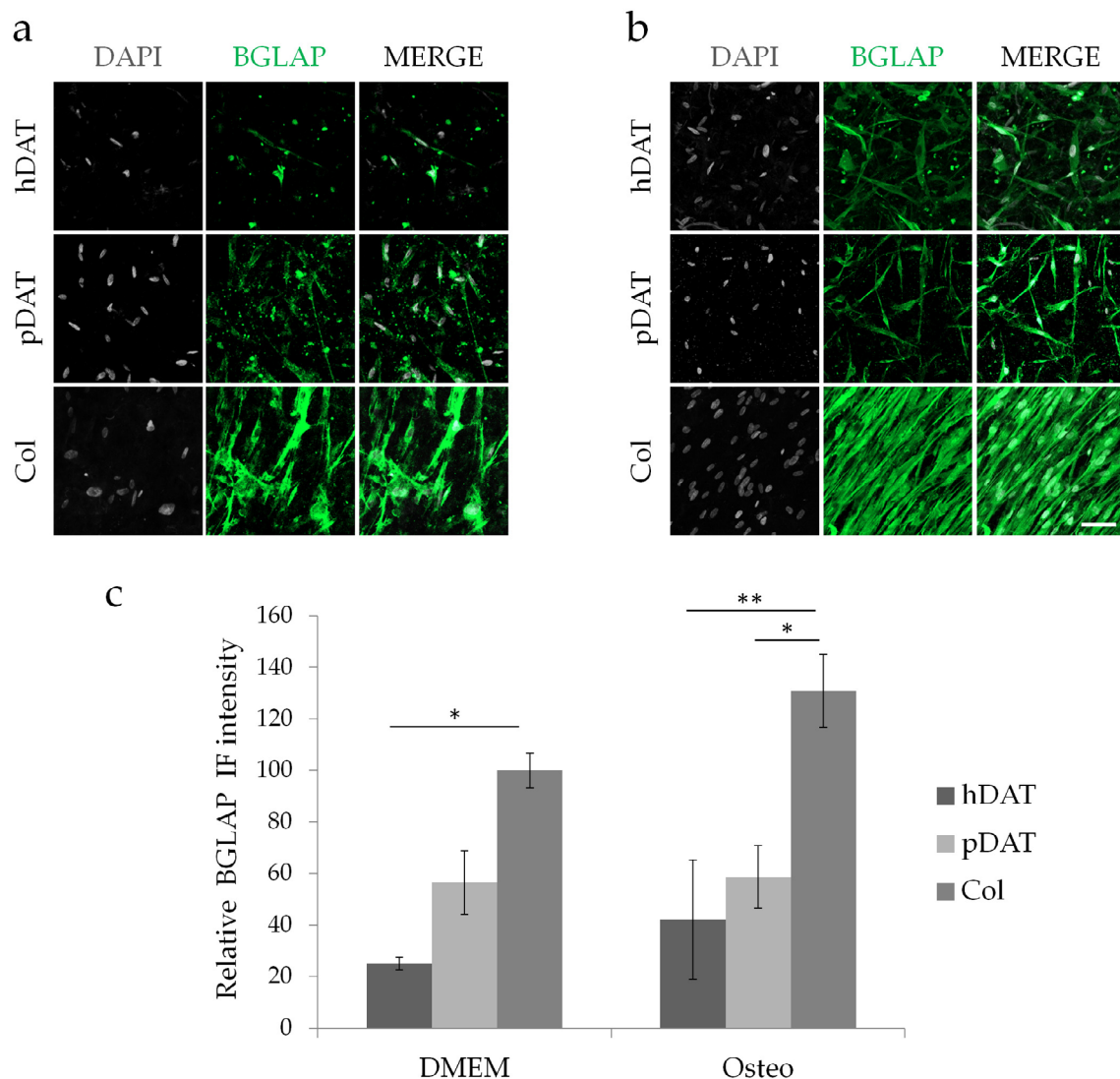


Fig. 8. Expression of osteocalcin/BGLAP in 3D hDPSC cultures with hDAT, pDAT and Col solid foams. Osteocalcin/BGLAP IF was assessed after 2 weeks in culture, using the three scaffolds with the same hDPSCs in parallel. (a) hDPSCs grown in control conditions. (b) hDPSCs grown in osteodifferentiation (Osteo) conditions. Scale bar: 50 μ m. (c) Quantification of BGLAP IF labelling by fluorimetry (excitation/emission: 480/525 nm), $n = 3-4$, * $p < 0.05$, ** $p < 0.01$, Dunn's *post-hoc*, Kruskal-Wallis.

for bone tissue-engineering applications (Chamieh *et al.*, 2016; Rico-Llanos *et al.*, 2021; Zhang *et al.*, 2018). However, very few alternatives exist to effectively regenerate non-calcified tendons and ligament tissues, whose main protein component is also Col (Zhao *et al.*, 2021). In the present study, two novel biological scaffold biomaterials obtained from porcine and human DAT (pDAT and hDAT) were produced and a different osteoinductive biological activity was observed. These biomaterials could be applied alone or in combination with Col to generate tailored bone and joint tissue reconstructions with a better functional clinical outcome.

The field of dental implantology has reached considerable levels of success, with overall implant survival rates of around 95 % 10 years post-loading (Moraschini *et al.*, 2015) and of almost 88 % 20 years post-loading (Chrcanovic *et al.*, 2018). Despite ever-improving results of dental implant osseointegration over the last decades, significant challenges remain.

One of the most important is the MBL, which is inevitably associated with implant loading, due to the great mechanical stress imposed to the alveolar bone in the absence of a functional PDL (Chrcanovic *et al.*, 2018; Coli and Jemt, 2021; Galindo-Moreno *et al.*, 2015). In theory, one of the most effective strategies to reduce MBL and peri-implantitis would be to reconstruct the PDL that naturally serves as the cushioning interface between the bone and the dental piece. However, PDL engineering and regeneration represents an extraordinary challenge (Lee *et al.*, 2020). Any PDL refilling material should be able to firmly anchor to both the implant and bone surface borders while at the same time being refractory to full calcification, to help preserving a highly vascularised tissue strip in between.

In the context of stem cell therapy applied to PDL regeneration, the most desirable scenario would be that seeded cells were derived from the patients themselves (autologous graft), which would not

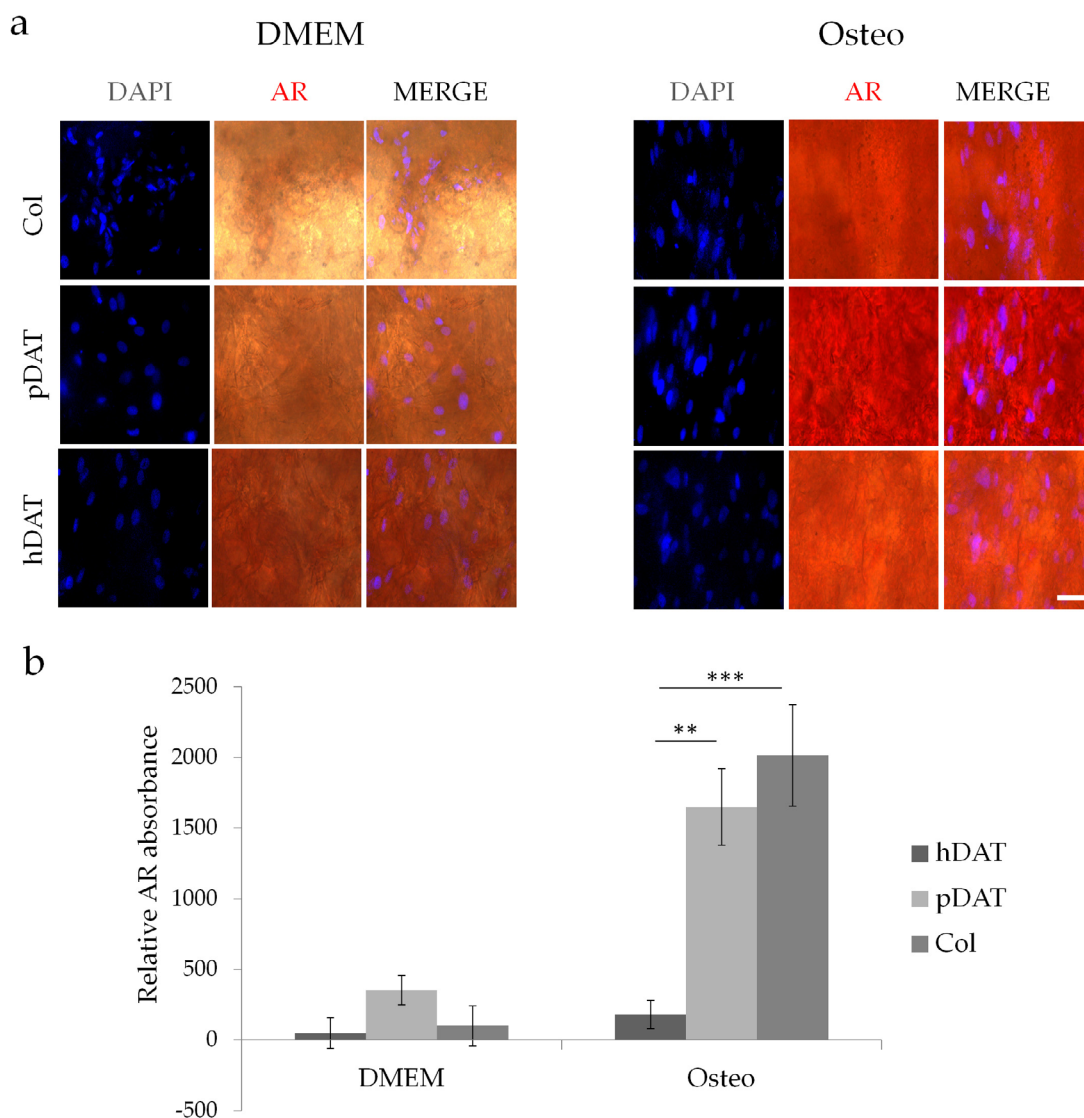


Fig. 9. Mineralised bone matrix production in 3D hDPSC cultures with hDAT, pDAT and Col solid foams. The production of calcified bone matrix was assessed by AR staining after 4 weeks in culture, using the three scaffolds with the same hDPSCs in parallel. **(a)** AR staining of 3D hDPSC cultures; nuclei in each frame were identified by DAPI counterstain. Scale bar: 50 μ m. **(b)** Photometric quantification of AR absorbance at 405 nm. $n = 3-5$, ** $p < 0.01$, *** $p < 0.001$, Tukey's *post-hoc* test, one-way ANOVA.

generate any immune rejection issue under adequate manipulation. Some of the most promising stem cell types for craniomaxillofacial cell therapy are hDPSCs, which are also particularly well suited for autologous transplant and cryopreservation (Aurrekoetxea *et al.*, 2015; Ibarretxe *et al.*, 2012; Raik *et al.*, 2020). Another great advantage of hDPSCs is that they can differentiate into a very large variety of both mesenchymal and non-mesenchymal cell types in the absence of xenogenic cell culture compounds such as animal serum. Importantly, hDPSCs are also known to differentiate towards both osteogenic and vasculogenic cells in serum-free media. A methodology to obtain vasculogenic cells (endothelia and pericytes) that does not involve the use of animal serum at any step was recently published and patented (Luzuriaga *et al.*, 2020; Web ref. 3). This method could be potentially applied to vascularise a large variety of scaffold materials, including pDAT and hDAT, for their use in tissue engineering therapies.

In the present study, hDPSCs were combined with ECM-derived porcine and human DAT solid foams,

following previously published decellularisation protocols (Brown *et al.*, 2011; Cicuéndez *et al.*, 2021; Web ref. 1). Both pDAT and hDAT materials showed excellent processing as 3D solid foams, with no significant differences in their structural properties. In the context of bone regeneration, it was very important to assess whether the integrated hDPSCs were able to differentiate towards osteoblastic cells within pDAT and hDAT. Significant differences were found at this level between hDAT and pDAT and/or Col. Results pointed to hDAT solid foam being a better scaffold for the regeneration of soft non-calcified tissues, whereas pDAT and Col solid foams would be more appropriate choices for mineralised bone regeneration. The results obtained supported the notion that pDAT and hDAT solid foams could constitute very interesting biomaterials for both hard- and soft-tissue engineering. The pDAT formulation sustained osteogenesis of hDPSCs to similar levels to Col, as assessed by ALP and AR staining. In contrast, hDAT scaffolds were much less permissive towards osteogenesis. Cells integrated well within the 3D scaffolds with no apparent loss of viability under

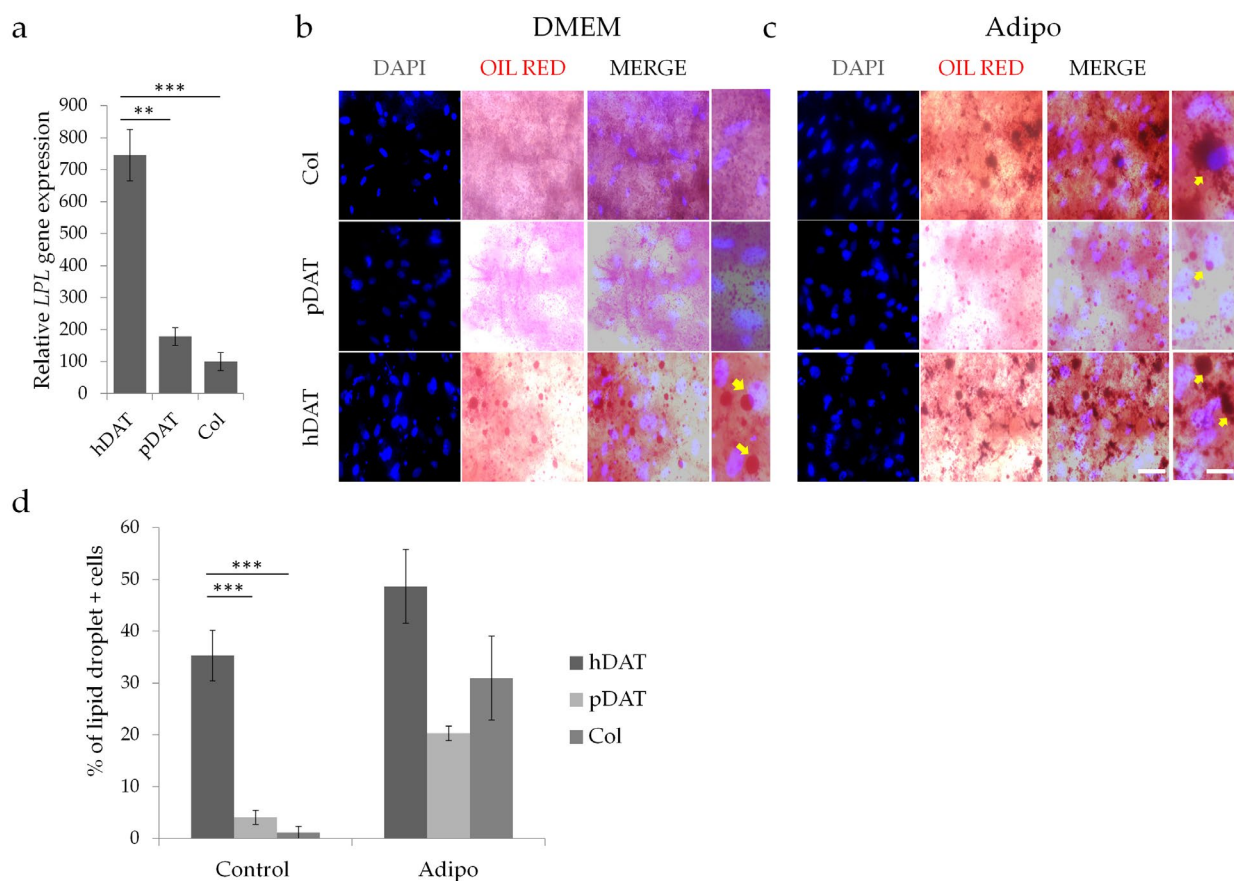


Fig. 10. Adipogenesis and lipid droplet production in 3D hDPSC cultures with hDAT, pDAT and Col solid foams. The three scaffolds were seeded with the same hDPSCs in parallel. (a) RT-qPCR analysis of *LPL* expression in hDPSC cultures at 2 weeks. $n = 3$, ** $p < 0.01$, *** $p < 0.001$, Tukey's *post-hoc* test, one-way ANOVA. (b) Lipid droplet production was assessed by oil red O staining after 4 weeks in culture. For these assays, hDPSCs were cultured for 4 weeks in both control (DMEM 10 % FBS; DMEM) and adipogenic differentiation enhancement conditions (DMEM 10 % FBS + IBMX, insulin, dexamethasone; Adipo). Cell nuclei close to lipid droplets are marked by yellow arrows. Scale bar: 50 μm (left-hand images) and 20 μm (right-hand images). (c) Quantification of the percentage of cells showing oil red O+ lipid droplets in each condition. $n = 5$, *** $p < 0.001$, Dunn's *post-hoc*, Kruskal-Wallis.

the conditions of the present study, where relatively low initial seeding densities (between 15,000 and 50,000 cells/well) and very small volumes of solid foams (approximately 200 $\mu\text{L}/\text{cm}^2$) were used. Sustaining higher cell loads over longer periods would probably require a better supply of oxygen and nutrients provided through a vascular network, which can be achieved under *in vivo* experimental conditions (Nakamura *et al.*, 2019). These *in vivo* experiments will be necessary to further assess the ability of hDAT and pDAT to enhance the healing of bone and associated soft tissue lesions.

Conclusions

DAT-derived biological scaffolds are very promising biomaterials for bone and soft tissue engineering. Both porcine and human DAT-derived materials provided a good substrate for hDPSC adhesion and viability. pDAT solid foams induced the osteogenic differentiation of hDPSCs to similar levels to Col. Osteogenesis in pDAT solid foams involved the production of calcified bone matrix by intramembranous ossification and the formation of Sharpey-fibre-like attachment structures. Interestingly, hDAT solid foams provided a different microenvironment from hDPSCs because 3D cultures in this material were refractory to mineralisation and had a higher adipogenic capacity. One of the main advantages of hDAT solid foams is that white AT is also a relatively abundant and an available source of human-derived raw-tissue material, which can be obtained from liposuction surgery. Given that both hDAT and hDPSCs can be isolated from human donors under ATMP standards, it could be interesting to combine them in personalised clinical therapies for the healing of bone and soft-tissue lesions.

Acknowledgements

This research was supported by the Basque Government (ELKARTEK program PLAKA KK-2019-00093; to NB), MICINN retos I+D+i (PID2019-104766RB-C21, to JRP) and UPV/EHU (PPGA20/22; to FU, GI). The authors would like to thank the staff members of the SGIKER services of the UPV/EHU: Lipidomic service (Beatriz Abad) and Analytical Microscopy (Ricardo Andrade, Alejandro Díez-Torre and Irene Fernández) for their technical assistance.

References

Aurrekoetxea M, Garcia-Gallastegui P, Irastorza I, Luzuriaga J, Uribe-Etxebarria V, Unda F, Ibarretxe G (2015) Dental pulp stem cells as a multifaceted tool for bioengineering and the regeneration of craniomaxillofacial tissues. *Front Physiol* **6**: 289. DOI: 10.3389/fphys.2015.00289.

Bertolini MM, Del Bel Cury AA, Pizzoloto L, Acapa IRH, Shibli JA, Bordin D (2019) Does traumatic occlusal forces lead to peri-implant bone loss? A systematic review. *Braz Oral Res* **33**: e069. DOI: 10.1590/1807-3107bor-2019.vol33.0069.

Bonnemain V, Thinarth R, Sergent-Tanguy S, Huet P, Bienvenu G, Naveilhan P, Farges J-C, Alliot-Licht B (2013) Human dental pulp stem cells cultured in serum-free supplemented medium. *Front Physiol* **4**: 357. DOI: 10.3389/fphys.2013.00357.

Brown BN, Freund JM, Han L, Rubin JP, Reing JE, Jeffries EM, Wolf MT, Tottey S, Barnes CA, Ratner BD, Badylak SF (2011) Comparison of three methods for the derivation of a biologic scaffold composed of adipose tissue extracellular matrix. *Tissue Eng Part C Methods* **17**: 411-421.

Chamieh F, Collignon A-M, Coyac BR, Lesieur J, Ribes S, Sadoine J, Llorens A, Nicoletti A, Letourneur D, Colombier M-L, Nazhat SN, Bouchard P, Chaussain C, Rochefort GY (2016) Accelerated craniofacial bone regeneration through dense collagen gel scaffolds seeded with dental pulp stem cells. *Sci Rep* **6**: 38814. DOI: 10.1038/srep38814.

Chrcanovic BR, Kisch J, Albrektsson T, Wennerberg A (2018) A retrospective study on clinical and radiological outcomes of oral implants in patients followed up for a minimum of 20 years. *Clin Implant Dent Relat Res* **20**: 199-207.

Cicuéndez M, Casarrubios L, Feito MJ, Madarieta I, Garcia-Urkia N, Murua O, Olalde B, Briz N, Diez-Orejas R, Portolés MT (2021) Effects of human and porcine adipose extracellular matrices decellularized by enzymatic or chemical methods on macrophage polarization and immunocompetence. *Int J Mol Sci* **22**: 3847. DOI: 10.3390/ijms22083847.

Coli P, Jemt T (2021) Are marginal bone level changes around dental implants due to infection? *Clin Implant Dent Relat Res* **3**: 170-177.

d'Aquino R, De Rosa A, Laino G, Caruso F, Guida L, Rullo R, Checchi V, Laino L, Tirino V, Papaccio G (2009) Human dental pulp stem cells: from biology to clinical applications. *J Exp Zool B Mol Dev Evol* **312B**: 408-415.

Diomede F, Marconi GD, Fonticoli L, Pizzicanella J, Merciaro I, Bramanti P, Mazzon E, Trubiani O (2020) Functional relationship between osteogenesis and angiogenesis in tissue regeneration. *Int J Mol Sci* **21**: E3242. DOI: 10.3390/ijms21093242.

Dzobo K, Motaung KSCM, Adesida A (2019) Recent trends in decellularized extracellular matrix bioinks for 3D printing: an updated review. *Int J Mol Sci* **20**. DOI: 10.3390/ijms20184628.

Franz-Odenaal TA, Hall BK, Witten PE (2006) Buried alive: how osteoblasts become osteocytes. *Dev Dyn* **235**: 176-190.

Galindo-Moreno P, León-Cano A, Ortega-Oller I, Monje A, O Valle F, Catena A (2015) Marginal bone loss as success criterion in implant dentistry: beyond 2 mm. *Clin Oral Implants Res* **26**: e28-e34.

Ge Q, Zhang H, Hou J, Wan L, Cheng W, Wang X, Dong D, Chen C, Xia J, Guo J, Chen X, Wu X (2018)

VEGF secreted by mesenchymal stem cells mediates the differentiation of endothelial progenitor cells into endothelial cells *via* paracrine mechanisms. *Mol Med Rep* **17**: 1667-1675.

Giuliani A, Manescu A, Langer M, Rustichelli F, Desiderio V, Paino F, De Rosa A, Laino L, d'Aquino R, Tirino V, Papaccio G (2013) Three years after transplants in human mandibles, histological and in-line holotomography revealed that stem cells regenerated a compact rather than a spongy bone: biological and clinical implications. *Stem Cells Transl Med* **2**: 316-324.

Gronthos S, Mankani M, Brahimi J, Robey PG, Shi S (2000) Postnatal human dental pulp stem cells (DPSCs) *in vitro* and *in vivo*. *Proc Natl Acad Sci U S A* **97**: 13625-13630.

Huang NF, Li S (2008) Mesenchymal stem cells for vascular regeneration. *Regen Med* **3**: 877-892.

Ibarretxe G, Crende O, Aurrekoetxea M, García-Murga V, Etxaniz J, Unda F (2012) Neural crest stem cells from dental tissues: a new hope for dental and neural regeneration. *Stem Cells Int* **2012**: 103503. DOI: 10.1155/2012/103503.

Irastorza I, Luzuriaga J, Martínez-Conde R, Ibarretxe G, Unda F (2019) Adhesion, integration and osteogenesis of human dental pulp stem cells on biomimetic implant surfaces combined with plasma derived products. *Eur Cell Mater* **38**: 201-214.

Jeon J, Lee MS, Yang HS (2018) Differentiated osteoblasts derived decellularized extracellular matrix to promote osteogenic differentiation. *Biomaterials Research* **22**: 4. DOI: 10.1186/s40824-018-0115-0.

Kabirian F, Mozafari M (2020) Decellularized ECM-derived bioinks: prospects for the future. *Methods* **171**: 108-118.

Keller PJ, Pampaloni F, Stelzer EH (2006) Life sciences require the third dimension. *Curr Opin Cell Biol* **18**: 117-124.

La Noce M, Mele L, Tirino V, Paino F, De Rosa A, Naddeo P, Papagerakis P, Papaccio G, Desiderio V (2014) Neural crest stem cell population in craniomaxillofacial development and tissue repair. *Eur Cell Mater* **28**: 348-357.

Langenbach F, Handschel J (2013) Effects of dexamethasone, ascorbic acid and β -glycerophosphate on the osteogenic differentiation of stem cells *in vitro*. *Stem Cell Res Ther* **4**: 117. DOI: 10.1186/scrt328.

Lee J-S, Kim S-K, Gruber R, Kim C-S (2020) Periodontal healing by periodontal ligament fiber with or without cells: A preclinical study of the decellularized periodontal ligament in a tooth replantation model. *J Periodontol* **91**: 110-119.

Luzuriaga J, Irurzun J, Irastorza I, Unda F, Ibarretxe G, Pineda JR (2020) Vasculogenesis from human dental pulp stem cells grown in matrigel with fully defined serum-free culture media. *Biomedicines* **8**: 483. DOI: 10.3390/biomedicines8110483.

Luzuriaga J, Pastor-Alonso O, Encinas JM, Unda F, Ibarretxe G, Pineda JR (2019a) Human dental pulp stem cells grown in neurogenic media differentiate

into endothelial cells and promote neovasculogenesis in the mouse brain. *Front Physiol* **10**: 347. DOI: 10.3389/fphys.2019.00347.

Luzuriaga J, Pineda JR, Irastorza I, Uribe-Etxebarria V, García-Gallastegui P, Encinas JM, Chamero P, Unda F, Ibarretxe G (2019b) BDNF and NT3 reprogram human ectomesenchymal dental pulp stem cells to neurogenic and gliogenic neural crest progenitors cultured in serum-free medium. *Cell Physiol Biochem* **52**: 1361-1380.

Luzuriaga J, Polo Y, Pastor-Alonso O, Pardo-Rodríguez B, Larrañaga A, Unda F, Sarasua J-R, Pineda JR, Ibarretxe G (2021) Advances and perspectives in dental pulp stem cell based neuroregeneration therapies. *Int J Mol Sci* **22**. DOI: 10.3390/ijms22073546.

Moraschini V, Poubel LA da C, Ferreira VF, Barboza E dos SP (2015) Evaluation of survival and success rates of dental implants reported in longitudinal studies with a follow-up period of at least 10 years: a systematic review. *Int J Oral Maxillofac Surg* **44**: 377-388.

Nakamura N, Ito A, Kimura T, Kishida A (2019) Extracellular matrix induces periodontal ligament reconstruction *in vivo*. *Int J Mol Sci* **20**. DOI: 10.3390/ijms20133277.

Ovchinnikov D (2009) Alcian blue/ alizarin red staining of cartilage and bone in mouse. *Cold Spring Harb Protoc* **2009**: pdb.prot5170. DOI: 10.1101/pdb.prot5170.

Pisciotta A, Riccio M, Carnevale G, Beretti F, Gibellini L, Maraldi T, Cavallini GM, Ferrari A, Bruzzesi G, De Pol A (2012) Human serum promotes osteogenic differentiation of human dental pulp stem cells *in vitro* and *in vivo*. *PLoS One* **7**: e50542. DOI: 10.1371/journal.pone.0050542.

Raik S, Kumar A, Rattan V, Seth S, Kaur A, Bhatta Charyya S (2020) Assessment of post-thaw quality of dental mesenchymal stromal cells after long-term cryopreservation by uncontrolled freezing. *Appl Biochem Biotechnol* **191**: 728-743.

Rico-Llanos GA, Borrego-González S, Moncayo-Donoso M, Becerra J, Visser R (2021) Collagen type I biomaterials as scaffolds for bone tissue engineering. *Polymers (Basel)* **13**: 599. DOI: 10.3390/polym13040599.

Sommer B, Bickel M, Hofstetter W, Wetterwald A (1996) Expression of matrix proteins during the development of mineralized tissues. *Bone* **19**: 371-380.

Uribe-Etxebarria V, Luzuriaga J, García-Gallastegui P, Agliano A, Unda F, Ibarretxe G (2017) Notch/Wnt cross-signalling regulates stemness of dental pulp stem cells through expression of neural crest and core pluripotency factors. *Eur Cell Mater* **34**: 249-270.

Uribe-Etxebarria V, García-Gallastegui P, Pérez-Garrastachu M, Casado-Andrés M, Irastorza I, Unda F, Ibarretxe G, Subirán N (2020) Wnt-3a induces epigenetic remodeling in human dental pulp stem cells. *Cells* **9**: 652. DOI: 10.3390/cells9030652.

Vasanthan KS, Srinivasan V, Pandita D (2021) Extracellular matrix extraction techniques and

applications in biomedical engineering. *Regen Med* **16**: 775-802.

Vimalraj S (2020) Alkaline phosphatase: structure, expression and its function in bone mineralization. *Gene* **754**: 144855. DOI: 10.1016/j.gene.2020.144855.

Wang L, Johnson JA, Zhang Q, Beahm EK (2013) Combining decellularized human adipose tissue extracellular matrix and adipose-derived stem cells for adipose tissue engineering. *Acta Biomater* **9**: 8921-8931.

Yang J-Z, Qiu L-H, Xiong S-H, Dang J-L, Rong X-K, Hou M-M, Wang K, Yu Z, Yi C-G (2020) Decellularized adipose matrix provides an inductive microenvironment for stem cells in tissue regeneration. *World J Stem Cells* **12**: 585-603.

Zhang D, Wu X, Chen J, Lin K (2018) The development of collagen based composite scaffolds for bone regeneration. *Bioact Mater* **3**: 129-138.

Zhao J, Wang X, Han J, Yu Y, Chen F, Yao J (2021) Boost tendon/ligament repair with biomimetic and smart cellular constructs. *Front Bioeng Biotechnol* **9**: 699. DOI: 10.3389/fbioe.2021.726041.

Web References

1. <https://patents.google.com/patent/WO2017114902A1/en> [22.02.2022]

2. <https://www.astm.org/Standards/F3354.htm> [22.02.2022]

3. <https://patentscope.wipo.int/search/en/detail.jsf?docId=WO2020007878> [22.02.2022]

Discussion with Reviewers

Juerg Gasser: Would you speculate on the factors that may explain the difference in osteogenic/adipogenic properties between pDAT and hDAT? Could the difference in rheological behaviour of the solid foams be a relevant factor or is the difference in molecular composition of the two foams more likely a major contributor?

Authors: Both the ECM stiffness and molecular composition could play a role in the DPSC differentiation process. Stiffer 3D ECMs tend to enhance osteogenic differentiation, whereas softer matrices promote adipogenic differentiation (e.g. Liu *et al.*, 2020; additional reference). The rheological behaviour of pDAT and hDAT did not show any statistical differences in viscoelasticity, only that pDAT retained more water than hDAT. Most native ECM and basement membrane proteins are conserved in both pDAT and hDAT, and protein composition of each material was described previously in detail (Cicuéndez *et al.*, 2021). In view of this, we are inclined to think that the adipogenic molecular cues that

are naturally present in the hDAT matrix could be more effective than those of pDAT when it comes to culturing human cells, due to a higher species-related homology.

Pierfrancesco Pagella: How do the authors envision the application of pDAT for the regeneration of human dental/periodontal tissues? Can the authors comment in more detail on the possible biocompatibility of porcine scaffolds with human tissue regeneration? See e.g. additional Web ref. 1.

Authors: The transplantation of porcine tissues and organs into humans to regenerate or replace irreversibly damaged body parts is an extremely interesting biomedical challenge, which is gradually becoming a reality. It is to be expected that the strategies to overcome xenotransplant-derived immune rejection will be increasingly refined over the next years and decades. In the case of pDAT, it must be pointed out that this biomaterial has been subjected to a decellularisation protocol, which should greatly reduce the chances of adverse immune reactions, compared to native non-decellularised porcine tissues. However, much work remains to be done to carefully characterise the possible immune rejection and clinical application of pDAT in humans. Regarding dental/periodontal regeneration, perhaps some of the most promising applications of these biomaterials could come from hDAT, which has shown a lower permissiveness than Col to sustain osteoblastic differentiation of DPSCs. This could be useful to regenerate soft dental tissues such as the periodontal ligament, which is lost as a consequence of dental extraction. Taking into account that hDAT constitutes a decellularised biomaterial and a clinically compatible human-derived product, it might eventually find a niche market in the context of upgraded dental implantology procedures.

Additional Reference

Liu Y, Li Z, Li J, Yang S, Zhang Y, Yao B, Song W, Fu X, Huang S (2020) Stiffness-mediated mesenchymal stem cell fate decision in 3D-bioprinted hydrogels. *Burns Trauma* **8**: tkaa029. DOI: 10.1093/burnst/tkaa029.

Additional Web Reference

1. <https://www.nature.com/articles/d41586-022-00111-9> [22.02.2022]

Editor's note: The Scientific Editor responsible for this paper was Thimios Mitsiadis.